International Journal of Fracture **119/120:** 449–474, 2003.
© 2003 *Kluwer Academic Publishers. Printed in the Netherlands.*

High-cycle fatigue of micron-scale polycrystalline silicon films: fracture mechanics analyses of the role of the silica/silicon interface

C.L. MUHLSTEIN* and R.O. RITCHIE*
Department of Materials Science and Engineering and the Materials Research Institute, The Pennsylvania State University, University Park, PA 16802 (E-mails: clm28@psu.edu; roritchie@lbl.gov)

Abstract. It is known that micron-scale polycrystalline silicon thin films can fail in room air under high frequency (40kHz) cyclic loading at fully-reversed stress amplitudes as low as half the fracture strength, with fatigue lives in excess of 10^{11} cycles. This behavior has been attributed to the sequential oxidation of the silicon and environmentally-assisted crack growth solely within the SiO_2 surface layer. This 'reaction-layer fatigue' mechanism is only significant in thin films where the critical crack size for catastrophic failure can be reached by a crack growing within the oxide layer. In this study, the importance of the bimaterial (e.g., Si/SiO_2) interface to reaction-layer fatigue is investigated, and the critical geometry and stress ranges where the mechanism is a viable failure mode are established.

Key words: Fatigue, MEMS, silicon, thin films.

1. Introduction

Although conventional theories would suggest that silicon should not fatigue at room temperature, several studies have now confirmed that micron-scale mono and polycrystalline silicon structural films, as used in microelectromechanical systems (MEMS), are susceptible to premature failure in cyclic fatigue in ambient atmospheres (Allameh et al., 2001; Bagdahn and Sharpe, 2002; Brown et al., 1997; Connally and Brown, 1992; Kahn et al., 1999; Kapels et al., 1999; Komai et al., 1998; Muhlstein et al., 2001a, b, 2002a, b; Tabib-Azar et al., 1992; Van Arsdell and Brown, 1999). This research, which has often involved electrostatically-actuated, notched, cantilever-beam fatigue test structures (Figure 1) to measure the stress-life (S/N) fatigue curves (Muhlstein et al., 2001a, b), has revealed that in room-temperature air, thin-film silicon ($\sim 2\ \mu$m thick) can exhibit 'metal-like' fatigue behavior with failures occurring at fully-reversed stress amplitudes of roughly one-half of the (single-cycle) fracture strength, after lives in excess of 10^{11} cycles (Figure 2). Recent studies by the authors have established that the mechanisms associated with such fatigue failures can be ascribed to a process of 'reaction-layer fatigue' involving the initiation, subcritical growth and catastrophic failure of nanoscale cracks within the native oxide layer (Figure 3) (Muhlstein et al., 2002a, b). Specifically, high-voltage transmission electron microscopy coupled with *in situ* monitoring of the compliance of the test structure to deduce crack sizes and oxide layer thicknesses, have shown that the native SiO_2 that initially forms on the silicon surface upon exposure to air (with a thickness and composition dictated by the environment and processing history) tends to thicken in the high stress regions (e.g., at the notch) during subsequent fatigue loading. This

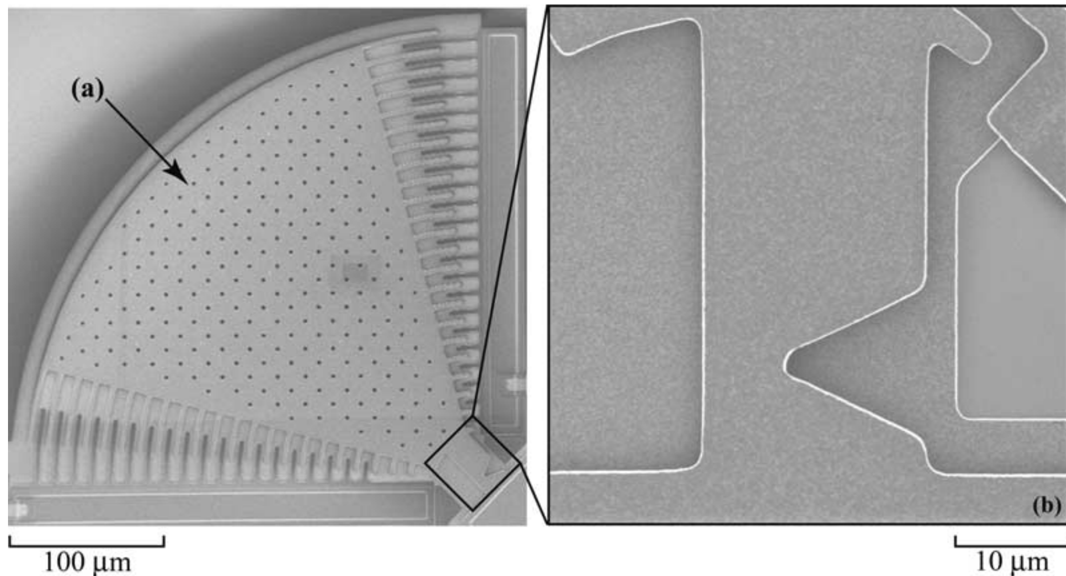

Figure 1. Scanning electron micrograph of the micron-scale fatigue characterization structure and the notched cantilever-beam specimen. The (a) toroidal mass and (b) notched cantilever-beam specimen (inset) are shown.

location then becomes the site for nanoscale cracks to initiate and grow due to the susceptibility of the silica to moisture-induced cracking[1]. Similarly, preexisting crack-like faults in the SiO_2 reaction layer may also grow during cyclic loading. The process then repeats itself until the critical crack size for failure of the entire test structure is reached, whereupon the silicon itself fractures catastrophically by transgranular cleavage (Muhlstein et al., 2002a, 2b). *The rate-dependence of thin-film silicon fatigue failures is thus dictated by the cycle-dependent oxide thickening process and the time-dependent, environmentally-assisted, crack initiation and subcritical growth in the oxide layer.*

The rate dependence of the reaction-layer fatigue process is invariably linked to the coupled interaction of the oxide layer growth and cracking within it. When the growth rates of the subcritical nanoscale cracks within the amorphous oxide layer were monitored (from the change in specimen compliance), they were found to be decreasing throughout most of the fatigue life (Muhlstein et al., 2002a, b). Such behavior was ascribed to several factors, most notably the likely presence of compressive residual stresses in the oxide layer and the fact that the cracks were propagating in a layered SiO_2/Si structure and approaching the SiO_2/Si interface. While the importance of residual stresses in understanding the driving force for crack advance is clear, the role of the bimaterial interface is less obvious. The presence of the compliant SiO_2 surface layer on the relatively stiff silicon structural film (polycrystalline silicon at room temperature has an elastic modulus nearly three times that of amorphous SiO_2) is known to lead to decreasing crack-driving forces that approach zero as the crack reaches the interface (Beuth, 1992). However, a more detailed fracture mechanics analysis is necessary to understand the importance of this bimaterial interface and the change in the local geometry induced by stress-assisted oxidation at the root of the notch to the evolution of fatigue damage

[1] In the absence of the native oxide layer, i.e., through the use of alkene-based monolayer coatings on the silicon surface, the susceptibility of thin-film silicon to cyclic fatigue failure has been shown to be markedly diminished (Muhlstein et al., 2002a, b).

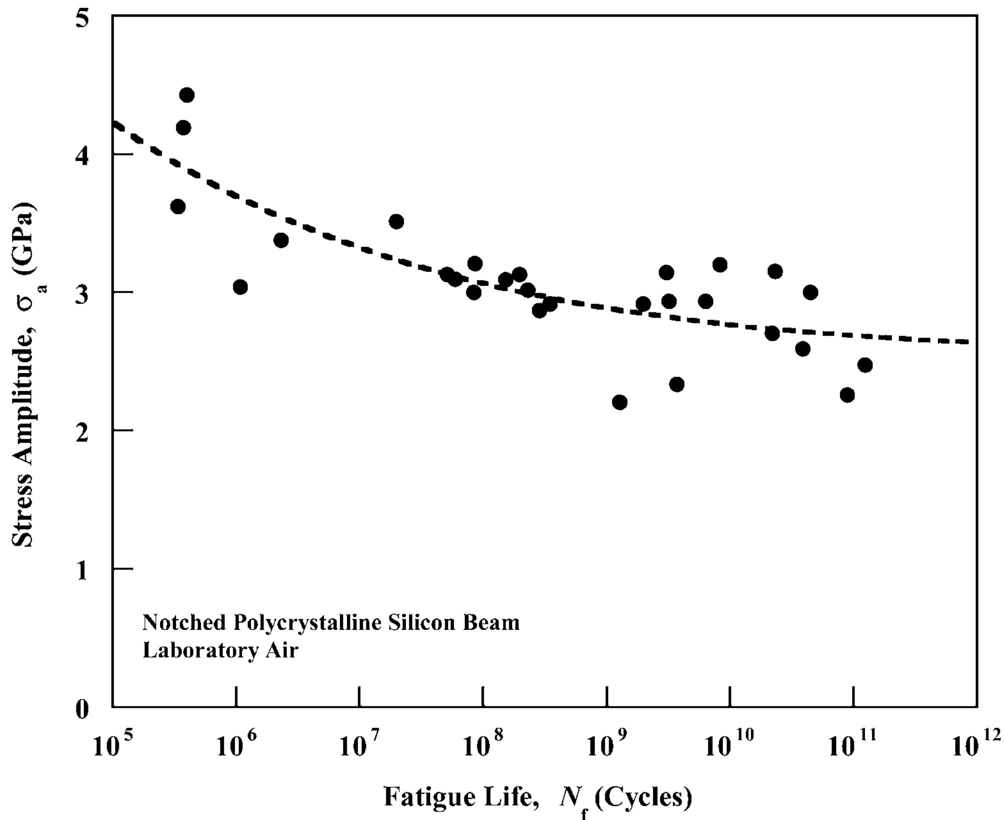

Figure 2. Stress-life (S/N) fatigue behavior of 2-μm thick polycrystalline silicon thin films at $\sim$40 kHz in laboratory air (Muhlstein et al., 2001a), determined using the thin-film fatigue characterization structure shown in Figure 1.

in polycrystalline silicon structural films. More importantly, materials other than silicon may be prone to reaction-layer fatigue if they form a surface reaction-layer (upon exposure to service or manufacturing environments) that is susceptible to environmental- or cycle-dependent cracking. *Specifically, the reaction-layer fatigue mechanism can lead to delayed failure of thin films of materials that are ostensibly immune to stress-corrosion cracking and fatigue in their bulk form.*

Accordingly, the objective of the present work is to establish the general requirements for reaction-layer fatigue and to apply this framework to establish the conditions for potential fatigue failure of polycrystalline silicon thin films. However, before establishing the design methodology, we first review some of the fundamental aspects of interfacial fracture mechanics, and then apply these elements to develop a general analytical approach for defining the regimes of susceptibility.

2. Interfacial fracture mechanics

The reaction-layer fatigue mechanism for silicon thin films suggests a configuration that involves cracks oriented normal to a bimaterial interface, within a surface layer, as shown schematically in the inset in Figure 4. The linear-elastic stress-intensity factor, K, for this

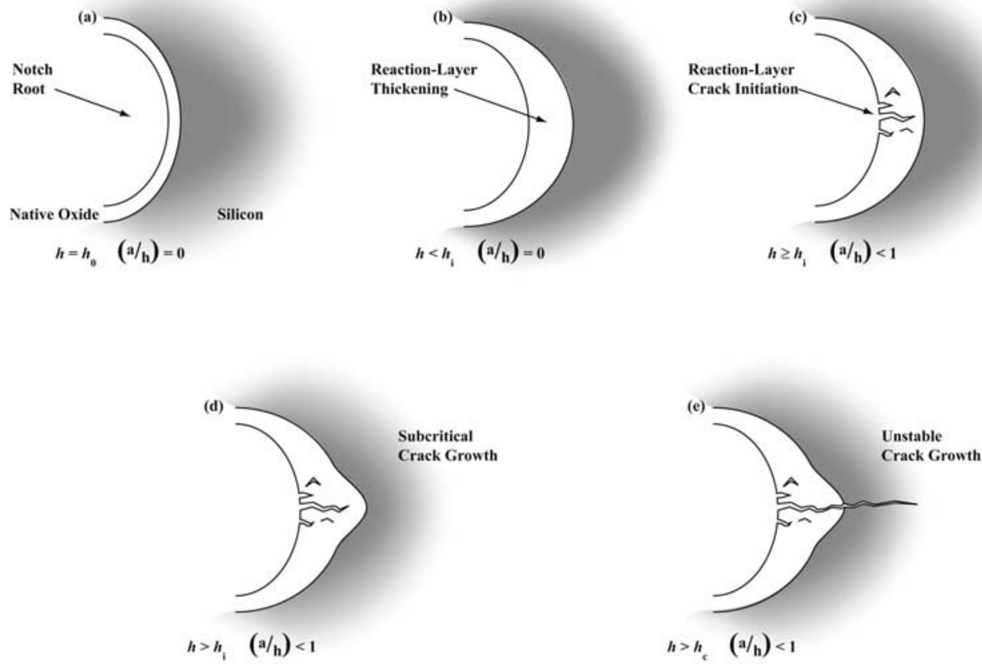

Figure 3. Schematic illustrations of the reaction-layer fatigue mechanism at the notch of the polycrystalline silicon cantilever beam. (a) Reaction layer (native oxide) on surface of the silicon. (b) Localized oxide thickening at the notch root. (c) environmentally-assisted crack initiation in the native oxide at the notch root. (d) Additional thickening and cracking of reaction layer. (e) Unstable crack growth in the silicon film. The thickness of the oxide, h, and relative crack size (a/h) at each stage of the reaction are shown.

configuration has been derived for cracks loaded in tension by the plane strain, biaxial stresses that can develop due to the mismatch in coefficient of thermal expansion between the layer and the substrate (Beuth, 1992; Gecit, 1979). Such interfacial solutions must be bounded at one extreme by the case of a surface crack of length, a, in a semi-infinite sheet, i.e., as $a/h \to 0$, $k \to 1.1215\sigma\sqrt{\pi a}$, where h is the layer thickness and σ is the applied stress. However, when the crack is near the interface (i.e., as $a/h \to 1$), the typical $1/\sqrt{r}$ stress singularity is not observed and the crack-tip stress field, σ_{ij}, is given by (Zak and Williams, 1963):

$$\sigma_{ij} \sim \widetilde{K} r^{-s} f_{ij}(\theta), \tag{1}$$

where $\widetilde{K}$ is analogous to the stress-intensity factor (with an appropriate change in units), r is the radial distance from the crack tip, $f_{ij}(\theta)$ is the angular distribution function, and s is the Zak–Williams singularity (Zak and Williams, 1963). In the absence of an elastic mismatch, $s = \frac{1}{2}$, as expected from monolithic fracture mechanics (see Anderson, 1995; Broek, 1986). However, the presence of a bimaterial interface can have a marked effect on the singularity and the associated crack-tip stress field. The strength of the Zak–Williams singularity is given by the root of:

$$\cos(s\pi) - 2\frac{\alpha - \beta}{1 - \beta}(1 - s)^2 + \frac{\alpha - \beta^2}{1 - \beta^2} = 0, \tag{2}$$

where α and β are the well-known Dundurs (1969) parameters, defined as:

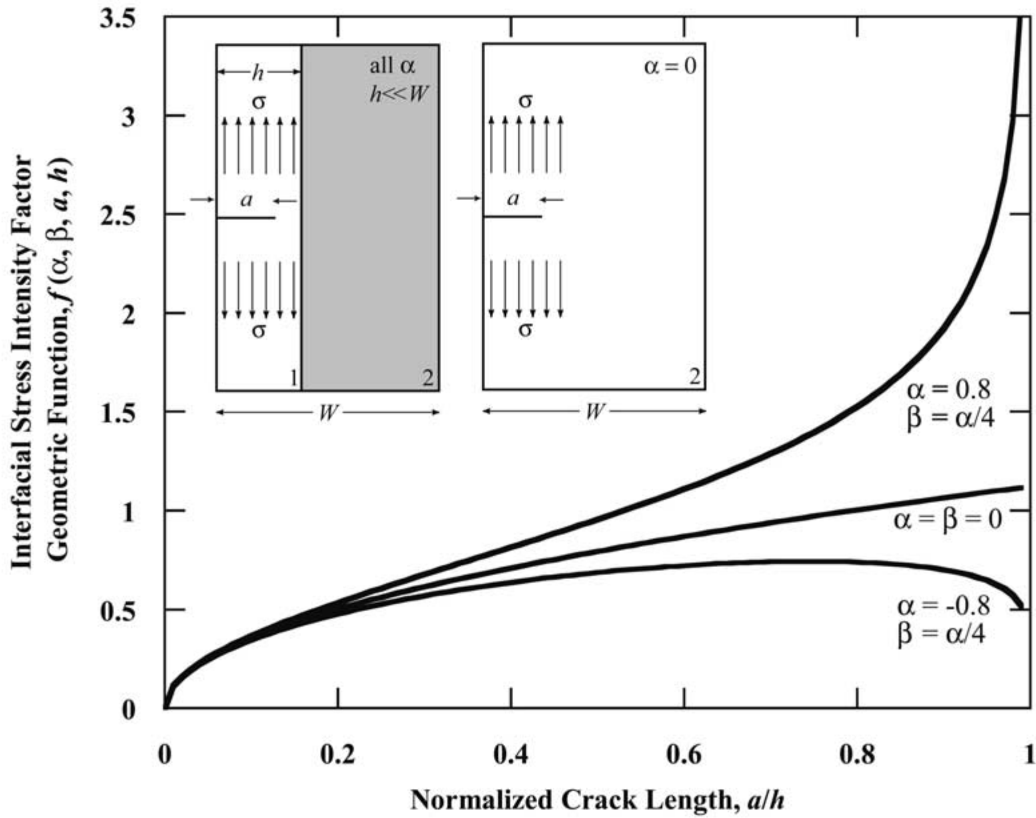

Figure 4. Schematic of the edge-crack in a surface loaded in tension and the general features of the solutions for the stress-intensity factor for a crack within a layer oriented normal to a bimaterial interface based on the general solutions, derived by Beuth (Beuth, 1992).

$$\alpha = (\overline{E}_1 - \overline{E}_2)/(\overline{E}_1 + \overline{E}_2),$$
$$\beta = \frac{\mu_1(1-2\nu_2) - \mu_2(1-2\nu_1)}{2\mu_1(1-\nu_2) + 2\mu_2(1-\nu_1)}. \quad (3)$$

In Equation (3), $\overline{E}_i \equiv E_i/(1-\nu_i^2)$ in plane strain and $\overline{E}_i \equiv E_i$ in plane stress, where E_i, μ_i and ν_i are, respectively, the Young's modulus, shear modulus and Poisson's ratio. The surface layer and the underlying substrate are denoted by the subscripts 1 and 2, respectively.

Consequently, the influence of the bimaterial geometry on the stress-intensity factor solutions for reaction-layer cracks enters calculations through the Dundurs parameters. The limiting cases of a short crack and a crack tip on the bimaterial interface have been analyzed by Beuth, who proposed the following general functional form for cracks contained within the surface layer (Beuth, 1992):

$$K_I \approx \sigma\sqrt{\pi h}\left(1.1215\left(\frac{a}{h}\right)^{1/2}\left(1-\frac{a}{h}\right)^{(1/2)s}\left(1+\lambda\frac{a}{h}\right)\right), \quad (4)$$

where λ is a curve-fitting parameter.

The general features of the linear-elastic stress-intensity factor solutions for cracks normal to an interface, within a surface layer, are shown in Figure 4. It is readily apparent that the

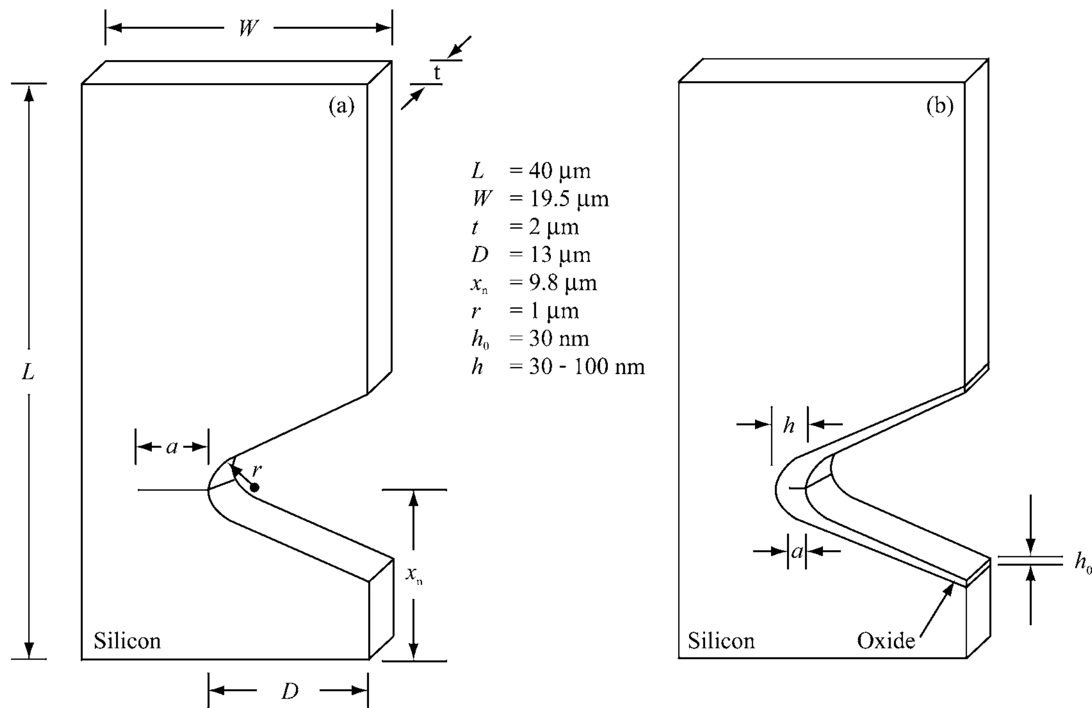

Figure 5. (a) Monolithic case: nominal dimensions and configuration of the notched cantilever-beam specimen in the electrostatically-actuation fatigue characterization structure used to evaluate the S/N fatigue behavior of polycrystalline silicon. (b) Bimaterial case: configuration of the initial thickness of the native oxide, h_O, notch root oxide thickness, h, and crack length, a, used in the oxidized structure models. The thickness of the oxide layer on the sides and root of the notch is exaggerated for clarity.

bimaterial case is a significant departure from the solutions for a monolithic (e.g., all silicon) structure:

$$K = \sigma\sqrt{\pi a}\, f(a/W), \tag{5}$$

where W is the width of the specimen, as shown in the inset in Figure 4. The elastic mismatch between the layer and substrate has a profound effect on the crack stability and driving force. For the case of a rigid film on a compliant substrate (i.e., $\alpha > 0$), the crack-driving force increases without bound as the crack approaches the interface; similarly, the driving force is continuously increasing when there is no elastic mismatch between the layers (i.e., $\alpha = 0$). However, for the case of a compliant film on a rigid substrate (i.e., $\alpha < 0$), the driving force for the crack displays a maximum at an intermediate value of normalized crack length, $(a/h)_{\max}$, after which the stress intensity decreases as the crack approaches the interface. These trends are observed over the range of β encountered in typical structural materials.

The stability of cracks within the layer can be determined using conventional fracture mechanics principles. One type of sample geometry that is capable of exploring these principles is seen in Figure 5. In the absence of resistance-curve behavior, a crack will begin to propagate when $K \geq K_c$ and will be unstable if $\mathrm{d}K/\mathrm{d}(a/W) > 0$ (Anderson, 1995; Broek, 1986). Analogous stability criteria can also be defined for fatigue-crack growth in terms of the stress-intensity range, ΔK. However, developing an unstable crack within the surface layer is a necessary, but not sufficient, requirement for catastrophic failure of the structure. In order to

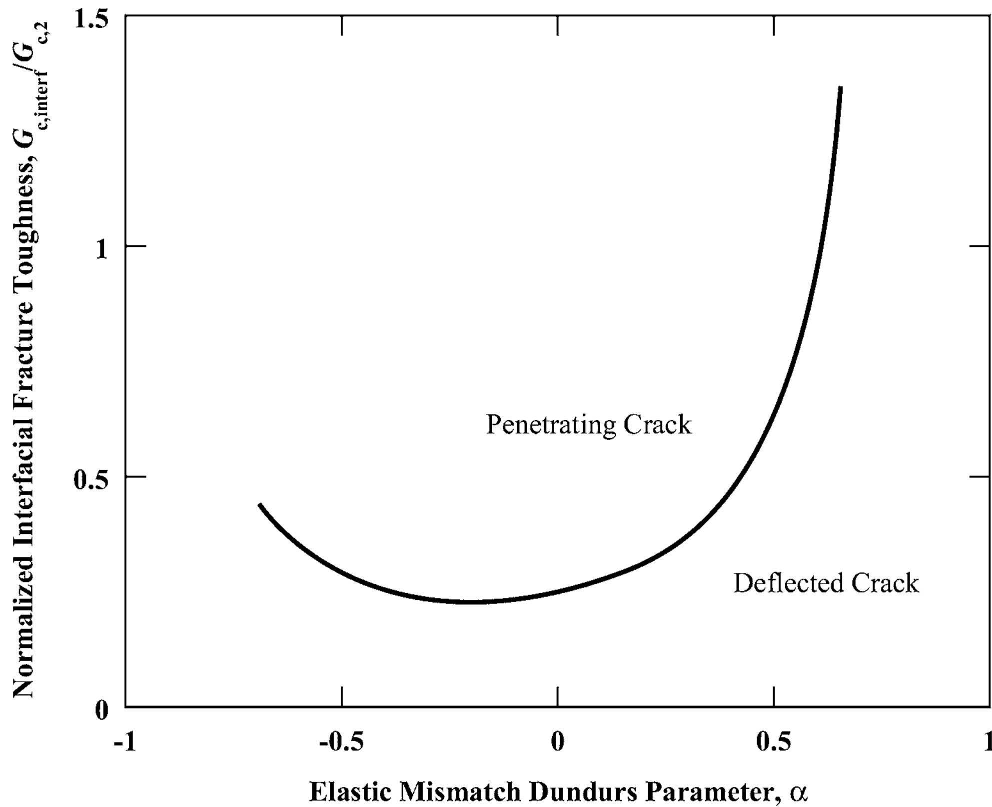

Figure 6. Linear-elastic conditions for the penetration or deflection of a crack normal to a bimaterial interface (after (He and Hutchinson, 1989)). The ratio of the fracture toughness of the interface, $G_{c,\text{interf}}$ to the fracture toughness of the underlying substrate, $G_{c,2}$, is shown as a function of the elastic mismatch Dundurs parameter, α. Since the behavior is a weak function of β, only the $\beta = 0$ case is shown. For normal impingement, when the interfacial fracture toughness is less than $\sim \frac{1}{4}$ that of the underlying substrate, the crack will be deflected by the interface.

predict catastrophic failure of a structure due to cracks normal to a bimaterial interface contained completely within the surface layer, it is necessary to consider the fracture toughness of the layer, $K_{c,1}$, interface, $K_{c,\text{int}}$ and the underlying substrate, $K_{c,2}$. Over-driven cracks in the layer may arrest at, be deflected at, or penetrate the interface depending on the relative fracture toughness of the substrate and the interface. The linear-elastic conditions for penetration and deflection of a crack at a bimaterial interface have been defined by He and Hutchinson (He and Hutchinson, 1989). In general, if the fracture toughness of the interface, expressed in terms of the strain-energy release rate G, is less than $\sim \frac{1}{4}$ of that of the underlying substrate, a crack normal to the interface will be deflected by that interface (Figure 6). Therefore, over-driven cracks will tend to penetrate the bimaterial interface and the conditions for catastrophic failure can be determined from the fracture toughness of the substrate except for the case of very weak interfaces. These general concepts of interfacial fracture mechanics, combined with conventional fracture mechanics for monolithic materials, can be used to develop a general framework for understanding the conditions required for reaction-layer fatigue.

3. Analysis methodology

In order for reaction-layer fatigue to occur, a specific set of conditions must prevail in the material systems as well as the particular geometry of the specimen/component. Cracks contained within the surface layer that reach a critical size must penetrate the bimaterial interface and continue to propagate. The initial phase of the analysis is to apply monolithic fracture-mechanics solutions to establish the critical crack sizes associated with the materials, applied stresses, and geometry of interest. If the critical crack sizes are commensurate with the reaction-layer thickness and the layer is susceptible to environmental- or cycle-assisted crack growth, further analysis using interfacial fracture mechanics solutions are necessary to assess the risk of failure due to reaction-layer fatigue. In order for catastrophic failure to occur due to a crack within the layer, the fracture toughness of the surface layer must be greater than, or (nearly) equal to, that of the substrate. Furthermore, the fracture toughness of the interface must be greater than some fraction of the substrate fracture toughness to insure that the crack will penetrate the interface (Figure 6). If these requirements are met for material combinations where $\alpha > 0$, cracks that initiate and grow within the surface layer will *always* reach a critical crack size and lead to catastrophic failure of the structure. However, if $\alpha < 0$, the presence of the intermediate maximum and subsequent decline in the stress-intensity factor leads to two possible outcomes. If the reaction layer is sufficiently thick and the applied stress large enough, a critical crack may develop. However, if the stress and/or layer thickness are too small, configurations can exist where cracks never reach a critical size within the reaction layer. The amorphous SiO_2 reaction layer on polycrystalline silicon substrates encountered in microelectromechanical systems falls into this latter category and will be explored at length in the following sections.

4. Numerical methods

The notched cantilever beams, used for thin-film fatigue testing at ~ 40 kHz (Figure 1), were ~ 40 μm long, 19.5 μm wide, and 2 μm thick. The notch was located 9.8 μm from the base and was 13 μm deep, with a root radius of approximately 1 μm, the smallest root radius that could be created given the processing conditions (Figure 5). The toroidal plate spanning 60° (inner radius, $r_{\text{inner}} = 30$ μm, outer radius, $r_{\text{outer}} = 300$ μm) rotates about the midpoint of the remaining ligament of the notched beam and serves as a mass to lower the natural frequency of the structure. A series of planar, finite element models of this structure were evaluated using a commercial software package (ANSYS v. 5.7). Quasi-static finite element models of the cracked, monolithic, notched cantilever beam were constructed and analyzed to determine the stress-intensity factor, K, and the nondimensional compliance, CEt (where C is the compliance, and t is the specimen thickness). In contrast to previous work (Muhlstein et al., 2003), these models focused on the extremely short cracks encountered in the stress-life fatigue behavior of Silicon films, i.e., for $a/(W - D) << 0.01$, where W is the width of the beam and D is the depth of the notch. Quasi-static analyses of cracked, *oxidized* silicon structures were also evaluated to determine the stress-intensity factor for a crack contained within the reaction layer. Modal analyses of both cracked and flaw-free, oxidized structures were used to establish the correlation between the natural frequency of the structure, which gives the compliance of the structure, and the evolution of fatigue damage in the form of notch-root oxidation and cracking of this oxide.

4.1. Monolithic solutions

In order to establish the range of applied stresses and geometries where reaction-layer fatigue is an important mechanism, fracture-mechanics solutions of the monolithic fatigue characterization structure may be used. It is appreciated that the actual case is bimaterial structure involving the cracking of a very thin reaction layer on top of a much larger and stiffer substrate, but the monolithic solutions do provide some useful insight.

The structure was modeled as an elastically isotropic, notched, cantilever beam and mass using six-node, triangular, plane-strain, solid elements with unit thickness. Small elastic deformations were assumed. The displacements of nodes located at the base of the notched cantilever beam were set to zero to achieve the 'built-in' boundary conditions of the structure. An average of the Voigt and Reuss bounds for a random, polycrystalline silicon aggregate (Young's modulus, $E = 163$ GPa, Poisson's ratio, $\nu = 0.23$ (Simmons and Wang, 1971)) was used for the elastic properties of the polycrystalline silicon elements. The density of the polycrystalline silicon, ρ in the modal analysis was assumed to be the same as the bulk, single crystal form ($\rho = 2329$ kg m^{-3} (Tatsumi and Ohsake, 1988)). The geometry of the mesh in the notch region was selected so that a direct comparison between the monolithic and bimaterial models was possible. The size of elements at the notch root and in the rest of the structure was refined until the solutions to the models converged. A subspace extraction method was used to determine the eigenvalues and eigenvectors for the system, establishing the first in-plane bending frequency and mode shape of the structure.

Modal and quasi-static structural analyses of cracked, notched, cantilever-beam structures were performed using the same material properties and finite element package as the crack-free structures using the geometry defined in Figure 5a. Akin to the uncracked structures, small deformations and elastic isotropy were assumed, displacements of nodes at the base of the cantilever structure were set to zero, and the material properties of an ideal polycrystalline silicon aggregate were used. The model of the characterization structure, with a crack located on the centerline of the notch (Figure 5a), was constructed with six-node, triangular, plane-strain elements. The singularity at the crack tip was modeled with twelve circumferential, unskewed elements. The size of the elements was 1/20 of the crack length or smaller. The size of the remaining elements was refined until the solutions to the model converged. As with the uncracked structure, a subspace extraction method was used to determine the eigenvalues and eigenvectors for the system, establishing the first in-plane natural frequency and mode shape of the structure. A unit force was applied at the center of mass of the plate in a direction perpendicular to the long axis of the beam and the stress intensity was then calculated from the displacement field immediately behind the crack tip (Anderson, 1995; Broek, 1986). The size of the crack was gradually increased to establish the stress-intensity geometric function, $f(a/(W - D))$, for the cracked structure using standard fracture-mechanics procedures (Anderson, 1995; Broek, 1986). The stress-intensity factor and nondimensional compliance were determined for structures with normalized crack sizes from ~ 0.0002 to 0.015, in order to focus the analysis on the range of crack sizes relevant to reaction-layer fatigue. A nonlinear, least-squares regression scheme using a Levenberg–Marquardt algorithm was used to fit a general form of a geometric function for the stress-intensity factor to the numerical results. A root-finding algorithm employing a combination of bisection, secant, and inverse quadratic interpolation methods (Forsythe et al., 1977) was used to establish the Zak–Williams singularity as well as critical values of crack size, oxide thickness, and other relevant parameters from the relationships developed from the finite element models and nonlinear regression.

4.2. INTERFACIAL SOLUTIONS

The oxidized fatigue characterization structure was modeled as an elastically isotropic, notched, bimaterial, cantilever beam and mass, with the geometry determined by scanning electron microscopy (SEM) of released devices, as summarized in Figure 5b. The SiO_2/Si interface was placed 46% of the oxide layer thickness *into* the silicon structural film to model the loss of silicon to the reaction layer during the oxidation process (Jaeger, 1993). Further oxidation from the initial native oxide thickness of 30 nm (Muhlstein et al., 2002a, b) was achieved by allowing the SiO_2/Si interface at the root of the notch to progress into the silicon and the SiO_2 outer surface to extend outward in a manner consistent with the consumption of silicon by the oxidation reaction. Six-node, triangular, plane-strain, solid elements with unit thickness were used in the model and small elastic deformations were assumed. The displacements of nodes located at the base of the notched cantilever beam were set to zero to achieve the ‘built-in’ boundary conditions of the structure. Akin to the monolithic structures, an average of the Voigt and Reuss bounds for a random, polycrystalline silicon aggregate was used for the elastic properties of the polycrystalline silicon elements and the density of the polycrystalline silicon, ρ in the modal analysis was assumed to be the same as the bulk, single crystal form. The material properties of the oxide layer were assumed to be the same as bulk, amorphous SiO_2 ($E \approx 60$ GPa, $\nu \approx 0.2$, $\rho \approx 2200$ kg m^{-3}). This bimaterial system is described by Dundurs parameters of $\alpha = -0.47$ and $\beta = -0.18$ and the corresponding Zak–Williams singularity of $s = 0.39$. The size of elements within the oxide layer was set to 7.5% of the notch root layer thickness and the remaining elements were refined until the solutions to the model converged. A subspace extraction method was used to determine the eigenvalues and eigenvectors for the system, establishing the first in-plane bending frequency and mode shape of the oxidized structure.

Modal and quasi-static structural analyses of cracked, notched, bimaterial, cantilever-beam structures were performed using the same material properties and finite element package as the crack-free structures. As with the uncracked structures, small deformations and elastic isotropy were assumed, displacements of nodes at the base of the cantilever structure were set to zero, and the material properties of an ideal polycrystalline silicon aggregate and amorphous SiO_2 layer were used. The model of the fatigue characterization structure with a crack within the oxide layer situated on the centerline of the notch (Figure 5b), was constructed with six-node, triangular, plane-strain elements. The singularity at the crack tip was modeled with twelve circumferential, unskewed elements. The size of the elements was either 1/20 of the crack length or 1/20 the remaining ligament, $(h - a)$, whichever was smaller. The size of the remaining elements within the oxide layer was set to 7.5% of the notch-root layer thickness and the rest of the mesh was refined until the solutions to the model converged. As with the uncracked structure, a subspace extraction method was used to determine the eigenvalues and eigenvectors for the system, establishing the first in-plane bending natural frequency and mode shape of the structure. A unit force was applied at the center of mass of the plate in a direction perpendicular to the long axis of the beam and the stress intensity was then calculated from the displacement field immediately behind the crack tip (Anderson, 1995; Broek, 1986). The size of the crack was gradually increased to establish the stress-intensity geometric function, $f(\alpha, \beta, a, h)$, for the cracked structure using standard fracture-mechanics procedures (Anderson, 1995; Broek, 1986). A nonlinear, least-squares regression scheme using a Levenberg–Marquardt algorithm was used to fit a general form of a geometric function for the stress-intensity factor to the numerical results. A root-finding algorithm employing a

combination of bisection, secant, and inverse quadratic interpolation methods (Forsythe et al., 1977) was used to establish the Zak–Williams singularity as well as critical values of crack size, oxide thickness, and other relevant parameters from the relationships developed from the finite element models and nonlinear regression. Finite element models of structures with notch root oxides thicknesses, h, varying from 30 to 100 nm were evaluated for relative crack sizes, a/h, from 0 to 0.95; these values were selected based on previously published experimental results for polycrystalline silicon structural films (Muhlstein et al., 2002a, b).

5. Results and discussion

5.1. Monolithic fracture mechanics analyses

We first consider the monolithic solutions and the critical crack sizes, a_c, associated with catastrophic failure of an edge-cracked sheet of polycrystalline silicon ($K_c \sim 1$ MPa $\sqrt{\text{m}}$) loaded in tension during S/N testing. Using conventional stress-intensity solutions from the literature (Tada et al., 2000), the computed values of a_c are plotted as a function of the applied stress, σ_{app}, in Figure 7a for various widths W of the sheet. The stress-life fatigue data in Figure 2 would suggest that, for lives less than $\sim 10^{11}$ cycles, the relevant, fully reversed stress amplitudes are in the range of ~ 2 to 5 GPa. For this range of stresses, it is apparent that the critical crack size for the micron-scale, thin-film silicon specimens is commensurate with the largest, experimentally measured oxide layer thickness ($h \sim 100$ nm) that forms under cyclic loading in ambient air (Muhlstein et al., 2002b). Since the oxide thickness is of the order of the critical crack size ($a_c \sim h$) for such sheet widths, i.e., typical of thin-film silicon, reaction-layer fatigue can be considered as a viable failure mechanism.

The monolithic solutions (provided they have the appropriate accuracy at very small normalized crack lengths) can thus be used to evaluate the relevance of the surface-layer failure mechanisms over the stress ranges of interest. Furthermore, these solutions can provide insight as to why the effect of reaction-layer fatigue is essentially insignificant for bulk silicon, consistent with the fact that there have been no reported instances of bulk silicon being susceptible to premature cyclic fatigue failures in ambient air environments. The calculations shown in Figure 7a can be represented in a more general form by normalizing the critical crack size by the thickness of the native oxide, h, and the applied tensile stress normalized by the (single-cycle) strength of the material, σ_{ult}, as shown in Figure 7b. For large specimens (e.g., W_1 in Figure 7b), the critical crack size for failure at stresses below σ_{ult} is much larger than the reaction-layer thickness. Reducing the size of the specimen, however, will eventually lead to critical crack sizes that are similar in size to the native oxide (e.g., $W < W_{\text{crit}}$ in Figure 7b), as depicted schematically in Figure 8. Since for bulk silicon, $a_c >> h$ at applied stresses less than σ_{ult}, cycle- and moisture-induced cracking of the oxide layer cannot lead to failure of the entire structure. While the plots in Figure 7 clarify the geometric requirements for reaction-layer fatigue, an alternative representation of the results provides additional insight.

A general failure map for susceptibility to reaction-layer fatigue can be generated by plotting the relative critical crack size, a_c/h, for a given applied stress as a function of the specimen size normalized by the thickness of the reaction layer, as shown in Figure 9. This map can be used to define the regimes where polycrystalline silicon may be subject to such premature failures:

- At very low stresses, extraordinarily thick oxide layers would be required to support a critical crack for failure. Since these thick layers cannot develop (even with stress-

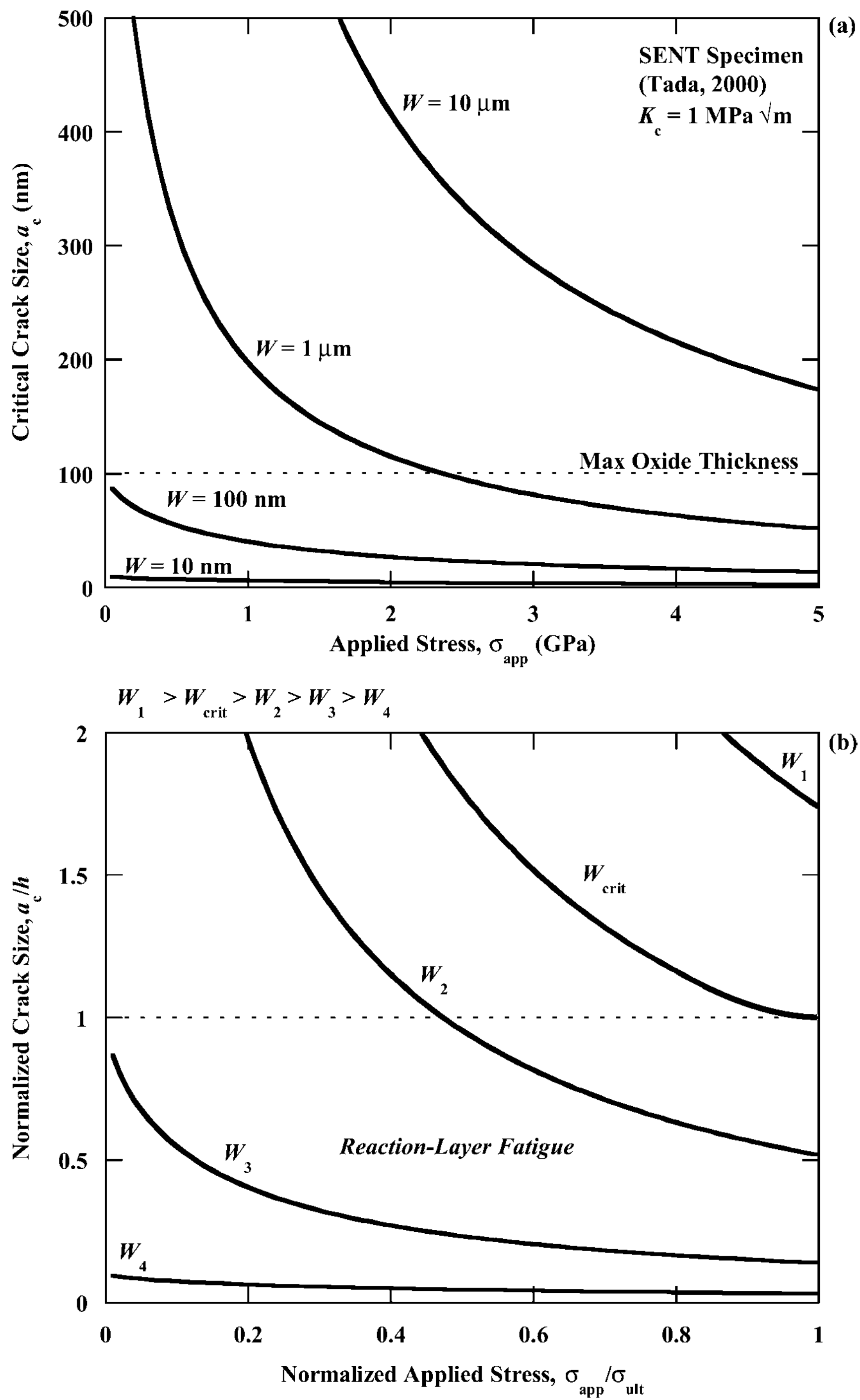

Figure 7. (a) Monolithic fracture mechanics estimate of the critical crack size, a_c, for a single-edge notched tension (SENT) (Tada et al., 2000) as a function of applied stress, σ_{app}, and specimen width, W, assuming a fracture toughness, K_c, of 1 MPa$\sqrt{\text{m}}$. The thickest, experimentally observed, native oxide in polycrystalline silicon is indicated for comparison. (b) General representation of the effect of specimen size, W, on the relevance of reaction-layer fatigue. For specimen sizes less than W_{crit}, reaction-layer fatigue may be observed since a_c is less than the notch-root oxide thickness, h.

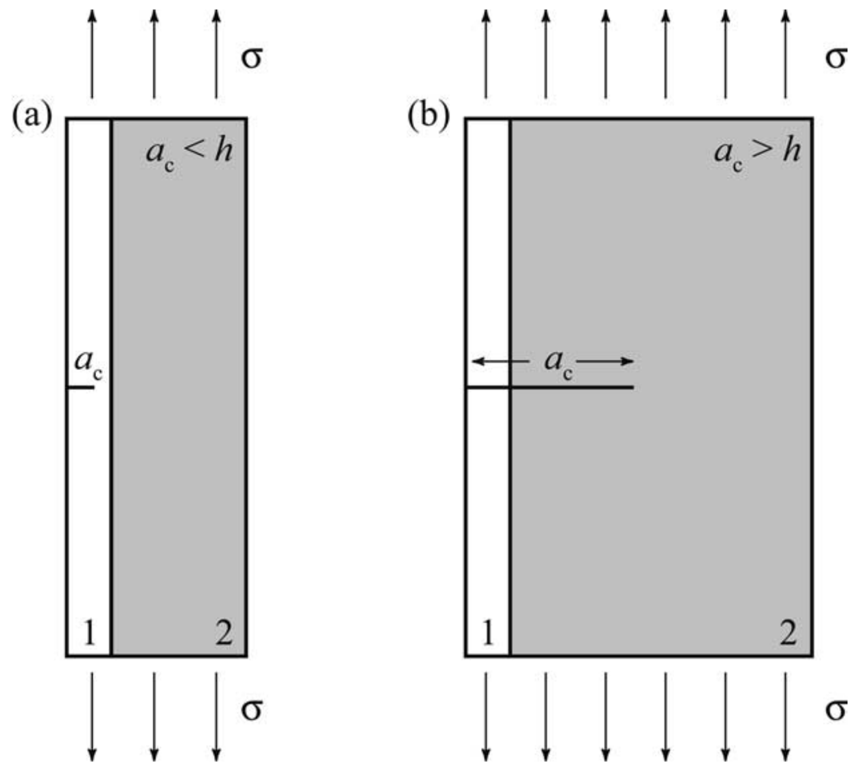

Figure 8. Schematic of the relative crack size for (a) thin film reaction-layer fatigue and (b) bulk behavior for silicon. When the critical crack size is of the same length scale as the oxide layer thickness, the fatigue mechanism is observed.

assisted oxidation), one would expect to see a threshold value below which reaction-layer fatigue should not be active.

- At intermediate stresses, two options appear to be possible. If the oxide layer is sufficiently thick, reaction-layer fatigue may occur. However, if the oxide thickness grows in service or during testing (as has been observed (Muhlstein et al., 2002a, b), the monolithic solutions suggest that increasing the reaction-layer thickness (while keeping the crack length constant) lowers the driving force for crack advance by reducing the relative crack size.[2] This, as well as the fact that there may be cracks within the native oxide that are not of a critical size, would suggest that subcritical crack growth should be possible and that not all cracks are capable of propagating to failure.
- Finally, at very high stresses, the strength of the material is exceeded and simply catastrophic failure occurs.

In previous studies of the notched cantilever-beam fatigue characterization structure, relative crack sizes from $a_c/h \sim 0$ to 0.85 were evaluated using finite element methods (Muhlstein et al., 2003). To facilitate a comparison with the interfacial models discussed below, additional monolithic fracture mechanics models of the characterization structure were evaluated in the present study for very short crack lengths, i.e., $a/(W - D) \ll 0.015$. The calculated values of the stress-intensity factor were recast in the standard functional form, and the geometric func-

[2]This conclusion is actually not correct and is an artifact of the monolithic solution, as shown in the following section.

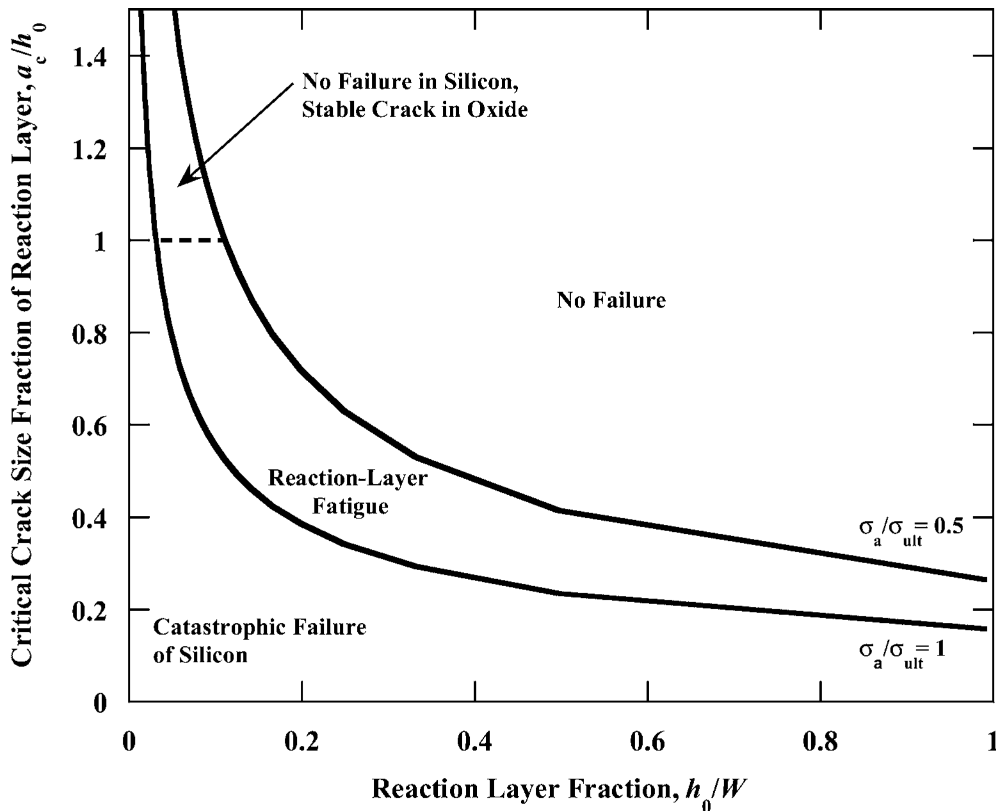

Figure 9. Bounds for reaction-layer fatigue calculated using the monolithic fracture-mechanics solutions. The critical crack size is shown as a fraction of the reaction-layer thickness for a given specimen size as a function of the applied stress. Note that several regions are predicted: (i) catastrophic failure of the silicon, (ii) reaction-layer fatigue, (iii) no failure, and (iv) stable cracking in oxide (no failure).

tion for the structure, $f(a/(W-D))$, shown in Figure 10, was fit to the following second-order polynomial expression:

$$f\,(a/(W-D)) = 1.9294 - 15.435\,(a/(W-D)) + 66.657\,(a/(W-D))^2 . \quad (5)$$

The nondimensional rotational compliance, $C_\theta Et$, for this structure (Figure 11) was then fit to the following second-order polynomial expression:

$$C_\theta Et = 4.2017 \times 10^{11} + 7.3858 \times 10^9\,(a/(W-D)) + 9.2573 \times 10^{12}\,(a/(W-D))^2 . \quad (6)$$

When these expressions are used to determine critical crack sizes over the range of stresses used during the stress-life fatigue tests (Figure 12), it is clear that they are again of the order of the thickness of the native oxide.

5.2. Interfacial fracture mechanics analyses

Using a bimaterial (amorphous SiO_2-polycrystalline silicon) finite element model of the notched cantilever-beam fatigue characterization structure (Figure 5b), the linear-elastic stress-intensity solutions were calculated and used to determine the geometric function for the interfacial crack as a function of crack size (Figure 13). It was found that the computed

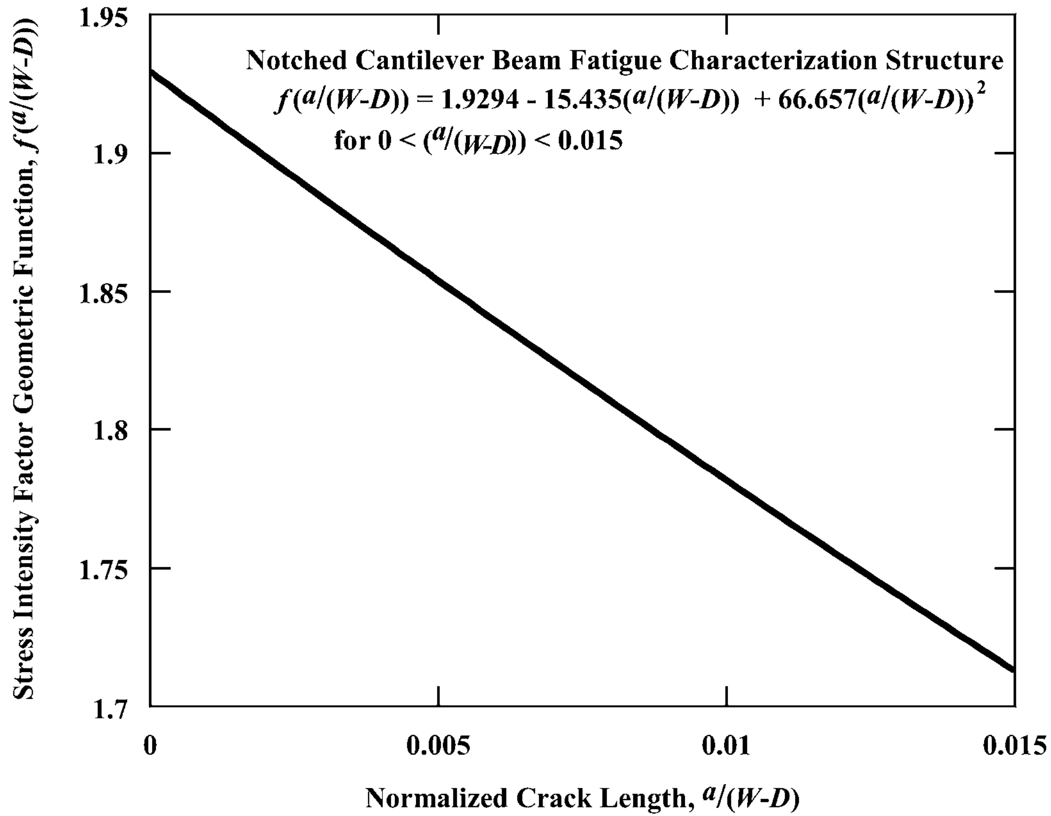

Figure 10. Stress-intensity factor geometric function for very short cracks ($a/(W-D) < 0.015$) in the notched cantilever-beam fatigue characterization structure.

mode II and III stress-intensity factors were orders of magnitude smaller than the mode I stress intensity. The geometric function for the stress-intensity factor, $f(\alpha, \beta, a, h)$, can be seen to exhibit an intermediate maximum $\left((a/h)_{\max} \approx 0.8\right)$ with increasing normalized crack size (Figure 13b). Cursory examination of the geometric function in the neighborhood of this maximum would (incorrectly) suggest that the influence of increasing oxide thickness on the stress-intensity factor changes depending on the value of normalized crack length. However, the $\sqrt{h}$ dependence shown in Equation (4) leads to an increasing stress-intensity factor with increasing oxide thickness. Attempts to fit this stress-intensity function to the general form in Equation (4) using nonlinear regression resulted in a low quality curve fit due to the differences between the geometry and loading conditions of the notched cantilever beam and the edge-cracked sheet analyzed by Beuth (1992). To improve the agreement between the fit function and the numerical data, the following modified form of the geometric function proposed by Beuth was used:

$$f(\alpha, \beta, a, h) = (m_h h + b_h)1.1215\left(\frac{a}{h}\right)^{1/2}\left(1 - \frac{a}{h}\right)^{(1/2)s}\left(1 + (m_\lambda h + b_\lambda)\frac{a}{h}\right), \tag{7}$$

where m_h, b_h, m_λ, and b_λ are curve-fit parameters. Nonlinear regression established values of 522244.2, 0.6389229, -1.043514×10^6 and -0.0268040 for m_h, b_h, m_λ and b_λ, respectively.

The interfacial K solutions for the notched cantilever-beam fatigue characterization structure have direct implications for understanding the cracking behavior encountered in reaction-

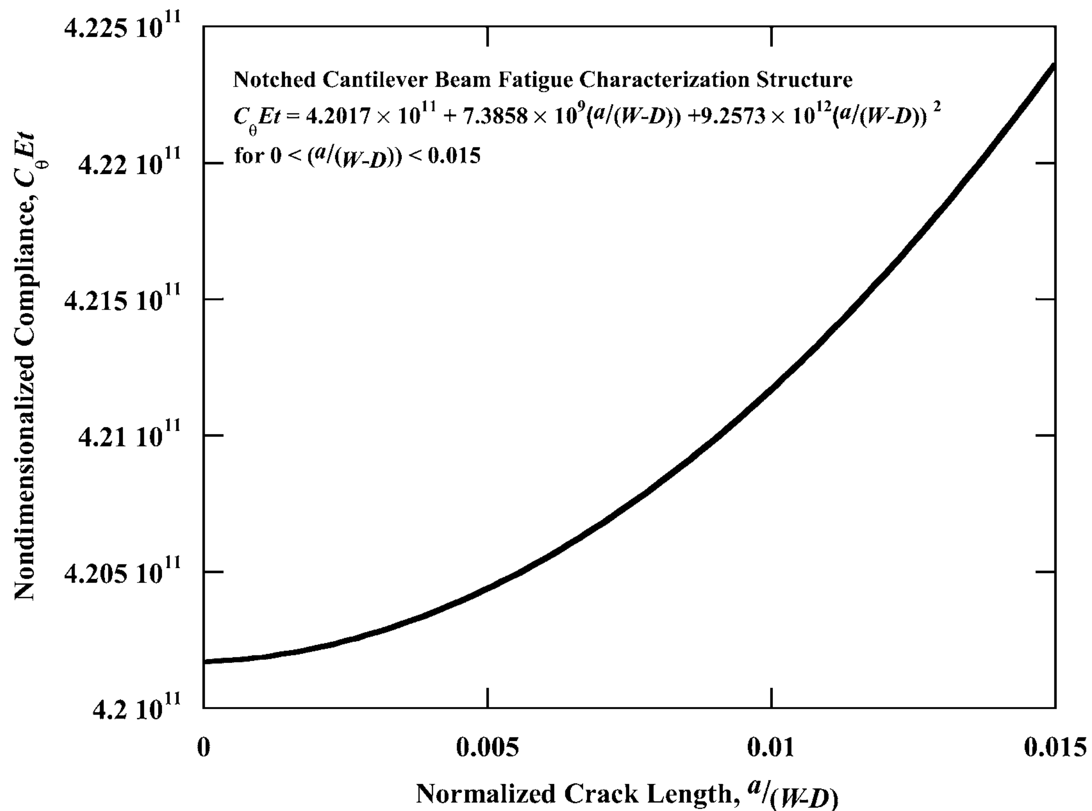

Figure 11. Nondimensional compliance, $C_\theta Et$, for very short cracks ($a/(W - D) < 0.015$) in the notched cantilever-beam fatigue characterization structure.

layer fatigue. A comparison of the crack-tip driving force for a particular thickness of oxide ($h = 100$ nm) highlights the influence of the interface. As expected from the general trends seen in the Beuth (1992) solutions, the presence of the interface between the compliant SiO_2 layer on top of the polycrystalline silicon substrate lowers the driving force for crack advance for a given applied stress and introduces an intermediate maximum in the variation of the stress-intensity factor with relative crack length (Figure 14).

An important aspect of the mechanics of the reaction-layer fatigue process is the relative importance of changes in crack length and oxide layer thickness on the driving force for crack advance. The geometric function in Figure 13 establishes that increasing the relative crack size leads to an intermediate peak in driving force that declines as the crack approaches the interface. Consequently, the derivative of the stress-intensity factor with respect to the relative crack size is positive, but decreasing, up to $(a/h)_{max}$ and becomes less than zero as the crack approaches the interface (Figure 15a). What is less obvious is the impact of the increase in the thickness of the oxide on the driving force for crack advance. Monolithic solutions suggest that increasing the oxide layer thickness (while maintaining a constant crack length) reduces the relative crack size and, hence, should reduce the stress-intensity factor (Figure 9). However, this is *not* the case. From the interfacial solutions it is apparent that increasing the thickness of the native oxide effectively pushes the influence of the bimaterial interface further away from the crack tip, thereby raising the driving force for crack advance. Consequently, the

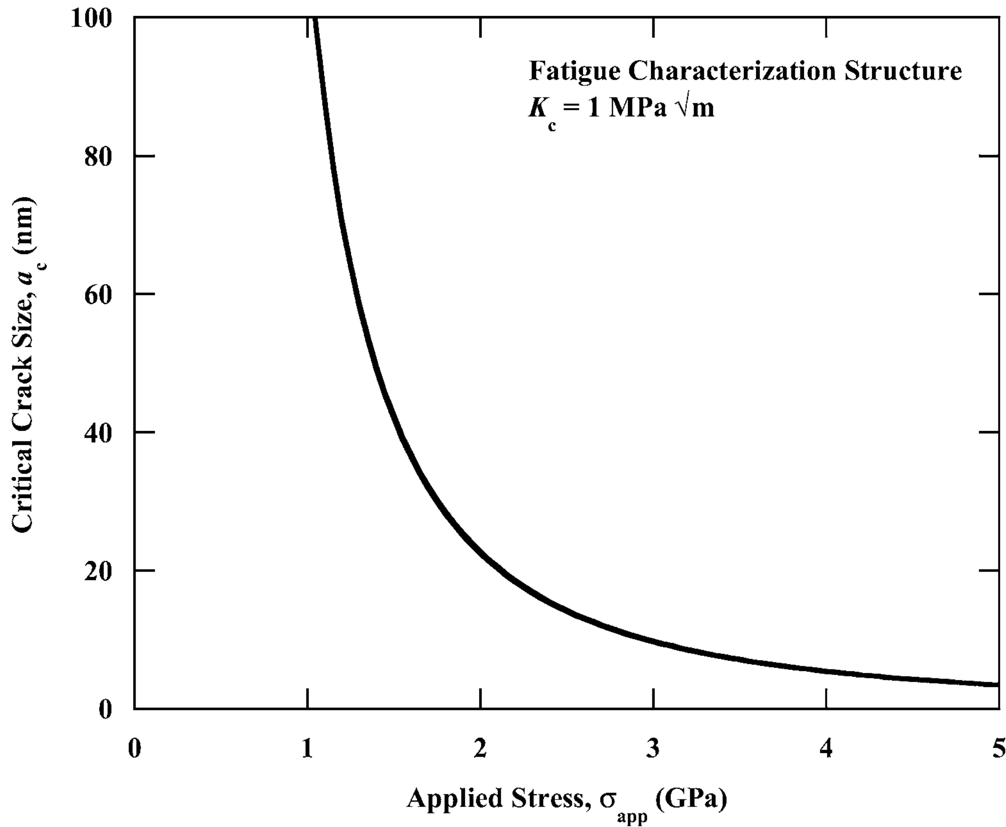

Figure 12. Estimated critical crack size, a_c, for the notched cantilever-beam fatigue characterization structure over the stress range used in S/N fatigue tests of polycrystalline silicon assuming a fracture toughness, K_c, of 1 MPa$\sqrt{\text{m}}$.

growth of the oxide layer, which occurs in the highly stressed notch region during reaction-layer fatigue, always leads to an increase in the driving force for crack advance, as illustrated in Figure 15b, since the gradient of the stress-intensity factor with respect to the oxide layer thickness is always positive. This key feature of the reaction-layer process is not captured by the monolithic K solutions.

In addition to reaction-layer fatigue, the presence of the intermediate maximum in the driving force for crack advance in the interfacial K solutions also has other important implications for the cracking patterns observed in thin films and the stability of channeling cracks (Hutchinson and Suo, 1992; Ye et al., 1992). In the case of the reaction-layer fatigue mechanism, the interfacial effect of the compliant oxide layer on top of the relatively stiff polycrystalline substrate sets discrete bounds for when the reaction-layer fatigue mechanism is expected to be active, i.e., when thin-film silicon may be susceptible to premature failure from this mechanism. Specifically, the crack driving force at $(a/h)_{\text{max}}$ represents the largest stress-intensity factor, K_{max}, that can be generated for a given geometry and applied stress when the crack length is less than the layer thickness (i.e. $a < h$).

Combining this understanding of the role of the oxide layer thickness and the intermediate maximum in the driving force for cracks within the layer provides a framework for defining when reaction-layer fatigue can occur in silicon. Figure 16 shows the effect of oxide layer

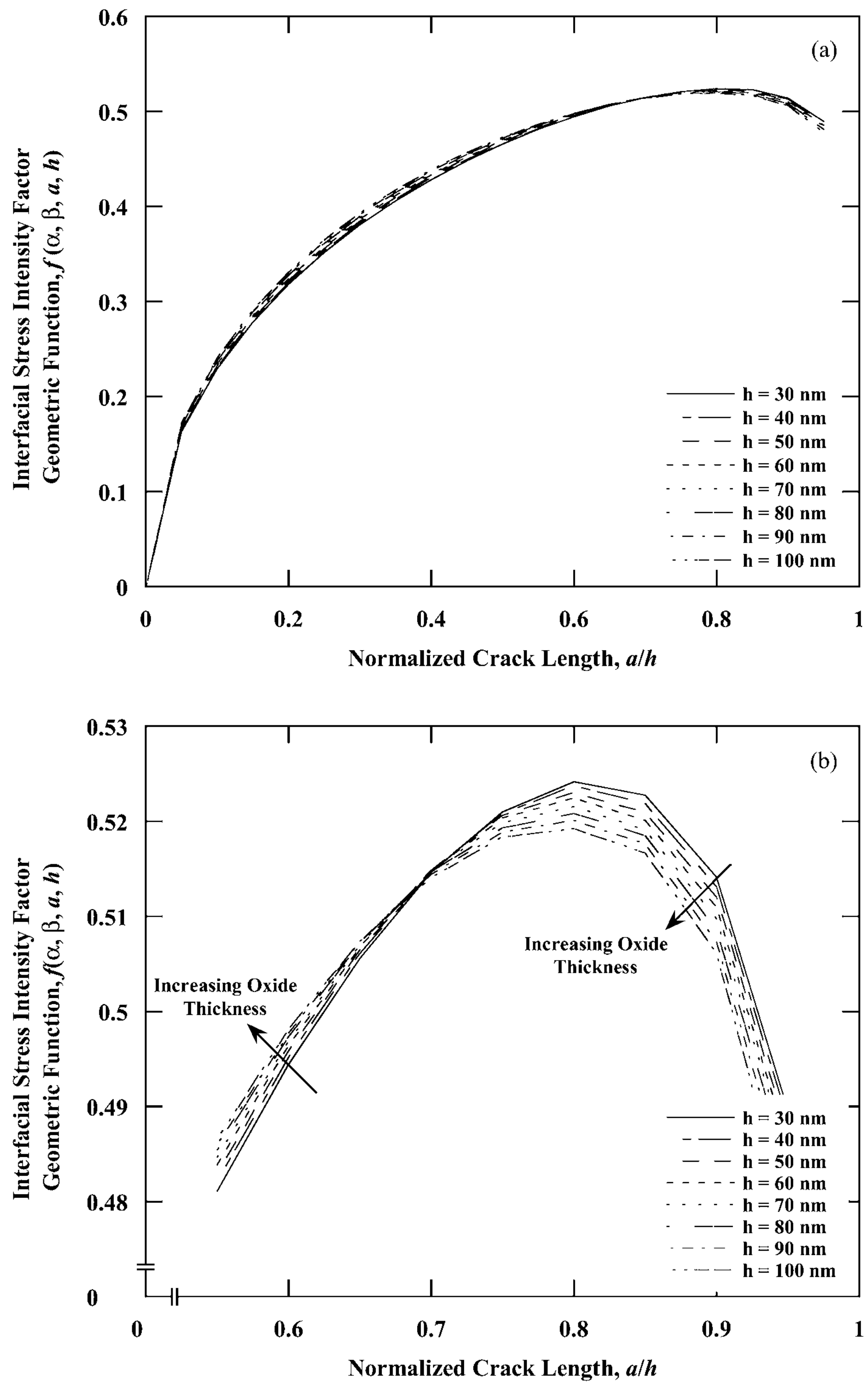

Figure 13. (a) The geometric function for the SiO_2-Si bimaterial case of the notched cantilever beam fatigue characterization structure derived from finite element models. The local oxide thickness at the notch root, h, was varied over the experimentally observed range of native oxide thickness (30 to 100 nm). (b) Detail of the geometric function in the vicinity of the local maximum illustrating the change in effect of increasing oxide thickness.

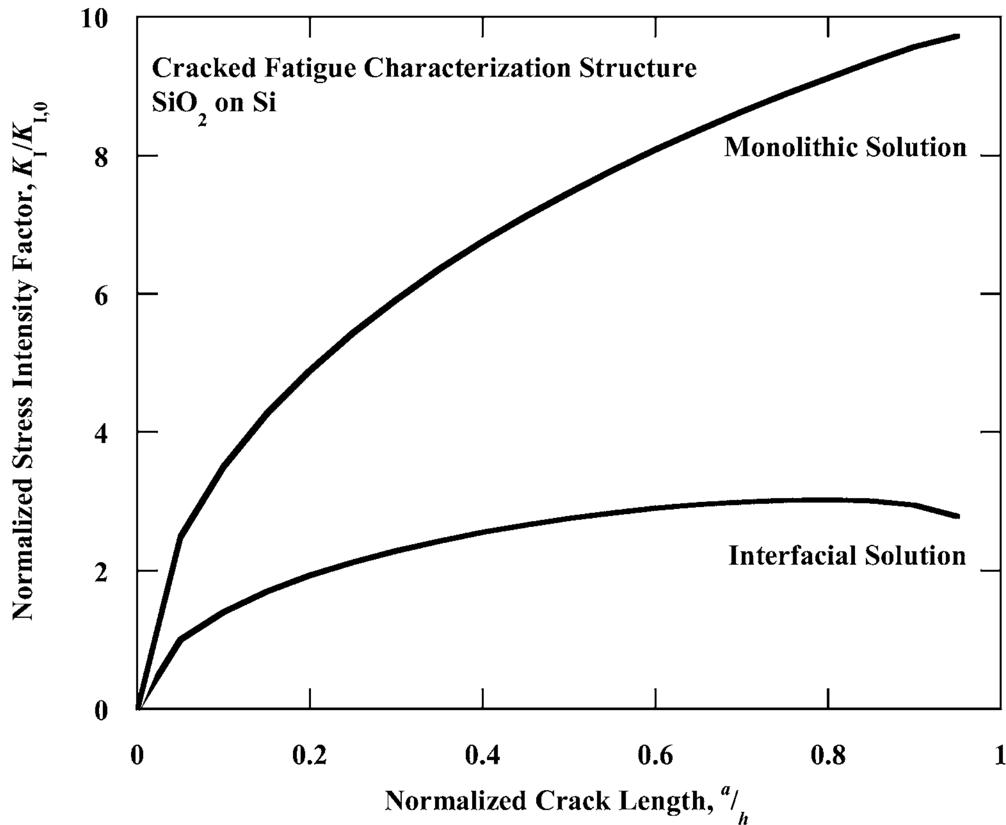

Figure 14. Comparison of the monolithic and interfacial solutions for the linear-elastic stress-intensity factor, K, for the notched cantilever-beam fatigue characterization structure. Note that (i) the presence of the amorphous SiO_2 layer on top of the polycrystalline silicon leads to a marked decrease in the driving force for crack advance under the same applied remote stress, and (ii) the interfacial solution exhibits a local maximum at $\sim a/h = 0.8$.

thickness and stress over the ranges observed experimentally in polycrystalline silicon. If the fracture toughness of the polycrystalline silicon ($K_c \sim 1$ MPa$\sqrt{\text{m}}$) and the environmentally-assisted cracking threshold for silica glass ($K_{\text{scc}} \sim 0.25$ MPa$\sqrt{\text{m}}$) are superimposed on the plot, it becomes evident that there is a minimum oxide thickness that must be present in order for cracks to *initiate* via environmentally-assisted cracking. What is less obvious is that these cracks can only reach a critical size (and cause failure of the entire structure) before reaching the bimaterial interface if the oxide layer is sufficiently thick. In order for failure to occur, the driving force for cracks growing within the native oxide must eventually exceed the fracture toughness of the material. If the oxide layer is too thin, the fracture toughness of the material cannot be reached for cracks within the surface layer of any size at stresses below the ultimate strength of the silicon. Given these solutions for the stress-intensity factor for cracks in the oxidized, notched, cantilever-beam specimen, we can calculate the critical value of oxide layer thickness required for crack initiation as a function of the applied stress (Figure 17). The critical initiation layer thickness, h_i, of 2.9 nm must exist in order to reach K_{scc} before the strength of the material is exceeded ($\sim$ 5 GPa). Therefore, it is relatively easy for cracks to be initiated in the reaction layers of thin-film silicon during fatigue since the native oxides encountered in the heavily-doped structural film are quite thick. This is an

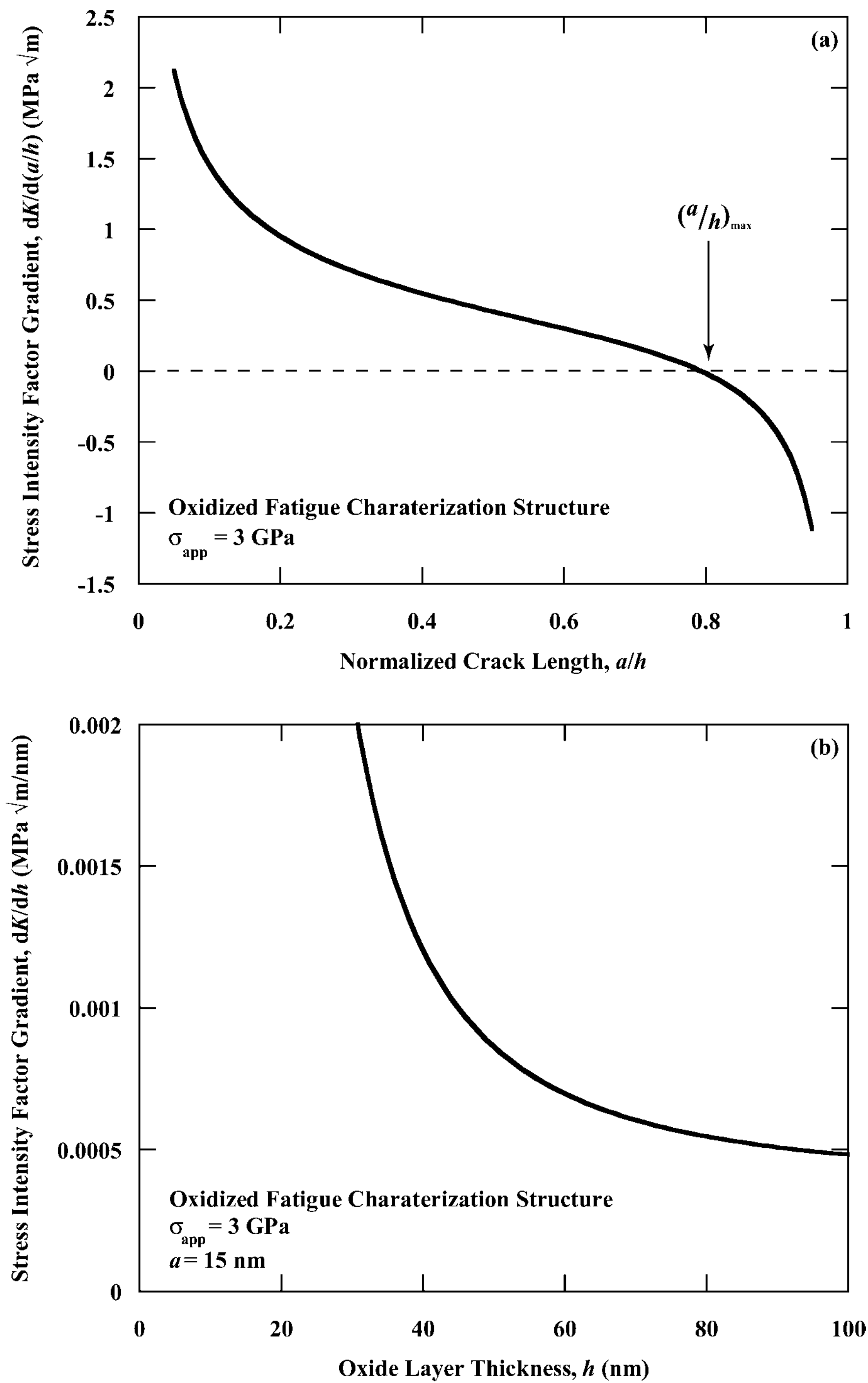

Figure 15. Effect of changes in oxide layer thickness, h, and the relative crack size, a/h, on the stress-intensity factor, K, for the amorphous SiO_2 on polycrystalline silicon notched cantilever-beam fatigue characterization structure. (a) The gradient of K with respect to the normalized crack length, a/h, shows that the driving force for crack advance is increasing until an intermediate point after which the driving force for crack advance decreases. (b) The gradient of K with respect to the oxide thickness indicates that increasing the oxide layer thickness increases the driving force for crack advance.

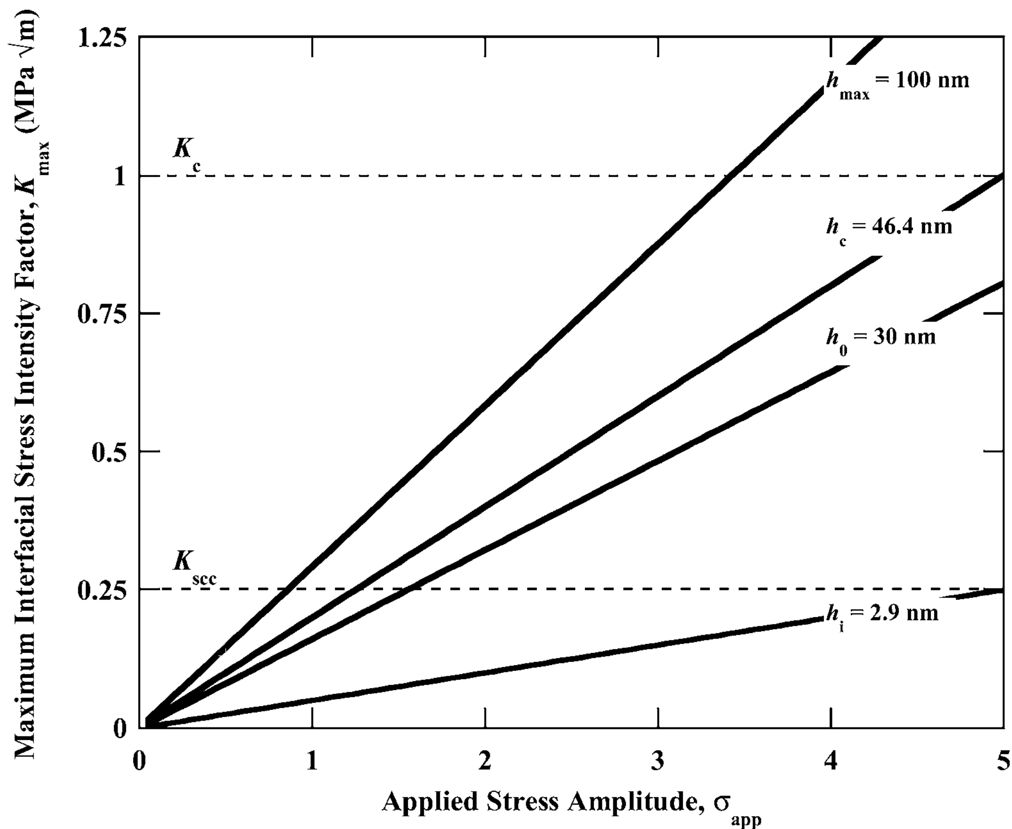

Figure 16. The effect of amorphous oxide layer thickness, h, on the maximum possible stress-intensity factor, $K_{\max}$, for a given applied stress amplitude, σ_{app}, in the polycrystalline silicon fatigue characterization structure. The critical initiation layer thickness, h_i, the initial native oxide thickness, h_o, the critical layer failure thickness, h_c, and the maximum reaction layer thickness observed in polycrystalline silicon, $h_{\max}$, are indicated on the plot. The threshold for environmentally-assisted cracking, K_{scc}, and the fracture toughness of the material, K_c, are shown for comparison.

interesting result since one might anticipate that steric hindrance (Michalske and Freiman, 1983), where the crack would not be sufficiently open to allow for environmentally-assisted cracking, might be a limiting case. Both intrinsic flaws in the oxide layer and those initiated by the synergistic interaction of the applied stress and the environment must be found within a sufficiently thick oxide layer, otherwise the fracture toughness of the layer cannot be exceeded and the component will never fail. For the polycrystalline silicon in our studies, a critical layer failure thickness, h_c, of 46.4 nm must be exceeded for a crack in the oxide layer to grow and exceed the fracture toughness of the material at stress levels below the strength of the material ($\sim$ 5 GPa).

It should be noted that these critical values of layer thickness are conservative. Whether a particular combination of applied stress and reaction-layer thickness could actually result in failure of the polycrystalline silicon should be determined from interfacial fracture-mechanics solutions (Figure 17). Depending on the stress range, there are very wide ranges of reaction-layer thickness for which environmentally-assisted crack initiation cannot occur and where cracks would never reach a critical size. This is presumably why the (relatively low stress) commercial applications of polycrystalline silicon MEMS are not currently plagued by fatigue

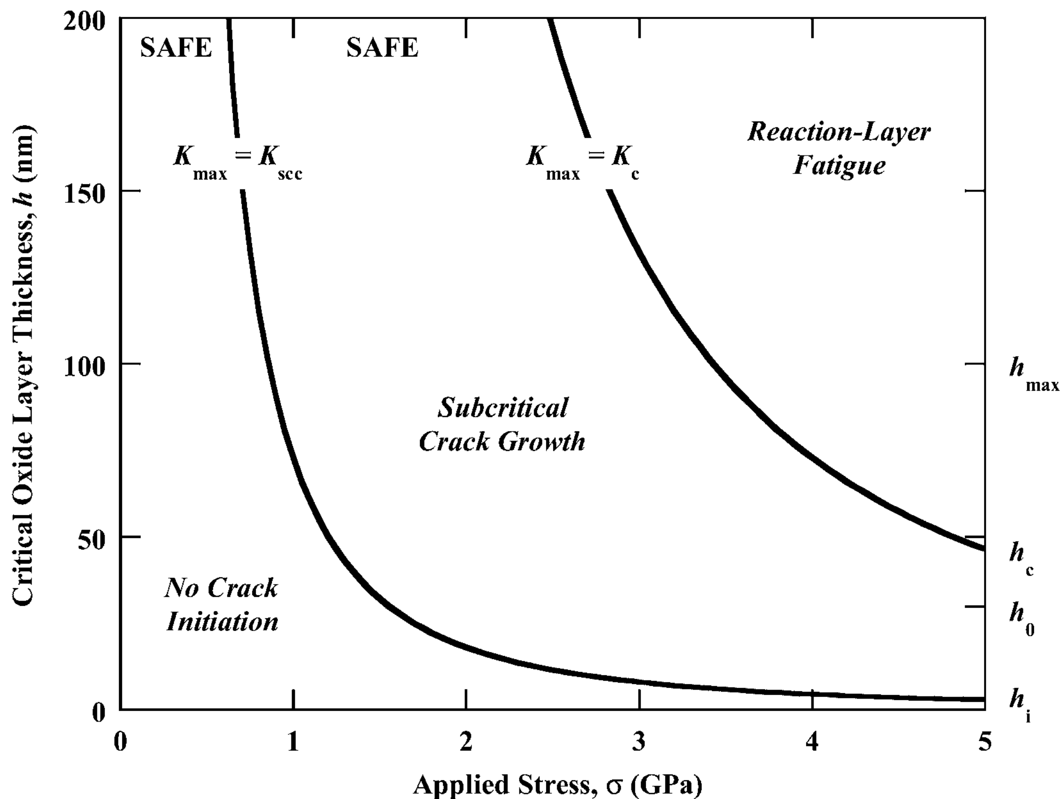

Figure 17. Critical oxide layer thickness for the reaction-layer fatigue mechanism. There are three regions associated with the reaction-layer fatigue mechanism. For a given maximum applied stress, there is a maximum oxide layer thickness below which cracks cannot initiate via environmentally-assisted mechanisms. At larger oxide layer thicknesses where the maximum driving force for the given applied stress does not exceed the fracture toughness of the material, cracks cannot propagate to failure. Finally, above a critical value of oxide layer thickness, reaction-layer fatigue failures can occur. The critical initiation layer thickness, h_i, the initial native oxide thickness, h_o, the critical layer failure thickness, h_c, and the maximum oxide thickness observed experimentally, $h_{\max}$, are indicated in the figure.

failures. However, this could well change when higher force actuators become available to MEMS designers.

5.3. Modal analysis

Stress-life fatigue data can be useful for engineers designing structures and for researchers interested in comparing the relative susceptibility of materials and the efficacy of microstructural and surface modifications. However, without fatigue-crack growth rate data, it is difficult to develop an understanding of the mechanisms of fatigue-crack initiation and growth. Compliance measurements are a convenient means of monitoring crack length during conventional crack-growth tests. In the case of micron-scale, resonant fatigue testing, the changes in specimen compliance manifest themselves as changes in the natural frequency of the specimen. The challenge lies in how to interpret these changes in specimen compliance.

Experimental evidence from (Muhlstein et al., 2002a, b) suggests that 'damage' in the form of stress-assisted oxidation as well as crack initiation and growth, occur in polycrystalline sil-

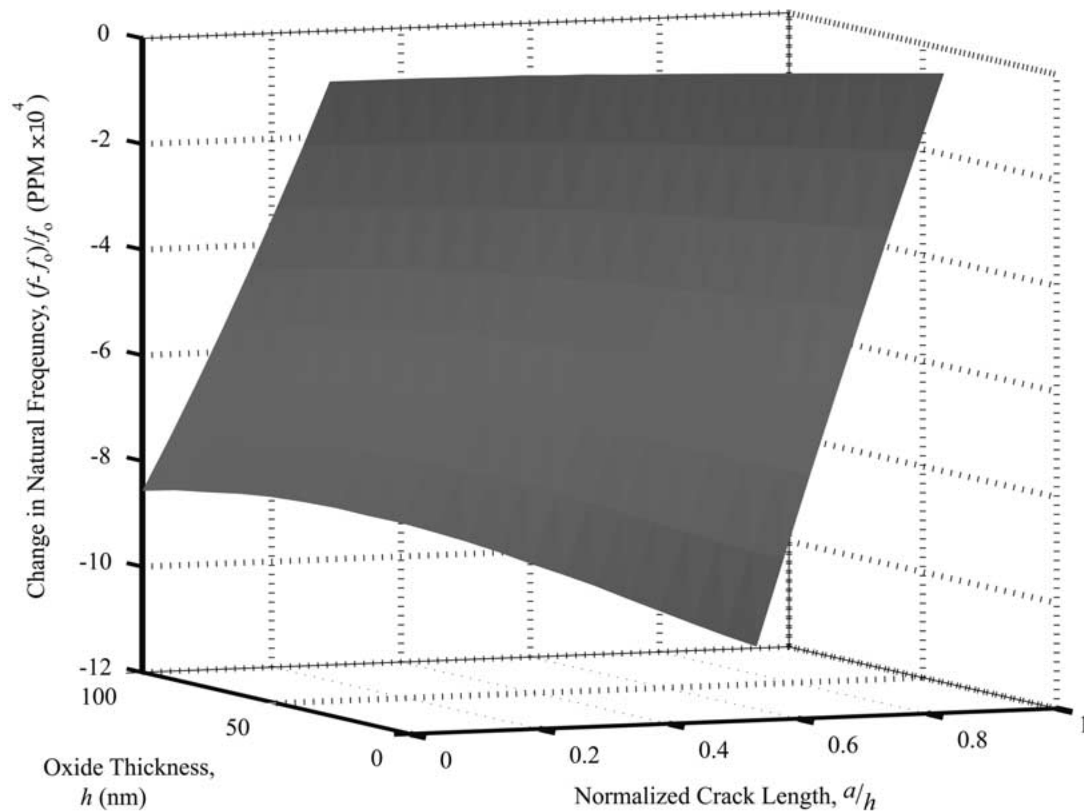

Figure 18. Three-dimensional surface representing the correlation between the specimen compliance, crack length, and oxide thickness.

icon during the reaction-layer fatigue process. Also, it is known that both notch root oxidation and cracking result in similar changes in specimen compliance (Muhlstein et al., 2001a). It is therefore necessary to have an understanding of the interrelationship between notch root oxidation and cracking of the specimen. To determine this relationship, finite element models identical to those used to determine the compliance and stress-intensity factor were evaluated. The resulting correlation between notch root oxidation and cracking and the compliance of the specimen is the surface shown in Figure 18. A given change in specimen compliance (i.e., the natural frequency) can be interpreted as a family of combinations of crack length and oxide layer thickness. The difficulty is to determine which geometry exists within the specimen at a given point in time. Fortunately, we do have some information on the initial and final configurations of the system. At the start of the test, a native oxide some 30 nm thick is present, and at the end of the test the notch root oxide thickness can (in principle) be measured for each specimen. However, the trajectory between these two points across the surface in Figure 18 is still undefined. Although experimental data exist that contain information on the crack and oxide layer growth rates, there is not sufficient information at present to use the measured changes in specimen compliance to separate these two phenomena in order to definitively establish fatigue-crack growth rates. Since the oxidation and cracking processes are likely coupled phenomena, this will probably require an independent measure of the crack length or the oxide thickness throughout the test to interpret the changes in compliance of the resonant fatigue characterization structure.

6. Summary and conclusions

Although it is generally accepted that micron-scale polycrystalline silicon thin structural films are susceptible to fatigue failure in room temperature air, the failure mechanism has until recently remained a mystery. Converging evidence has suggested that the failure of such silicon films is due to a sequential process of stress-assisted oxidation and environmentally-assisted cracking of the native oxide layer, a process that is termed reaction-layer fatigue. Since it is apparent that the entire process of crack initiation and crack growth up to the onset of catastrophic failure occurs within this oxide layer, and not the silicon itself, interfacial fracture-mechanics solutions defining the variation in crack-driving force, e.g., the stress-intensity factor, with change in crack size provide additional insight into the nature of this fatigue mechanism. There is a critical distinction between reaction-layer fatigue and environmentally-assisted crack growth mechanisms such as film-induced cleavage (Newman et al., 1989; Pugh, 1985) and slip dissolution (Ford and Silverman, 1979) where local crack advance halts at or near the bimaterial interface and the critical crack size is large compared to the reaction-layer thickness. Most importantly, the reaction-layer mechanism is one that can lead to delayed failure in thin films of materials that are ostensibly immune to stress-corrosion cracking and fatigue in their bulk form.

Based on fracture-mechanics solutions for the monolithic silicon and interfacial solutions for the SiO_2/Si layered structure, both for standard geometries and for the notched cantilever-beam fatigue characterization structure used by the authors, the following specific conclusions may be made:

1. Monolithic fracture-mechanics solutions can be used to establish when components are small enough that the reaction-layer fatigue phenomenon is a viable failure mode. Micron-scale (as opposed to bulk) structures are susceptible to reaction-layer fatigue because the critical crack size for failure is comparable to the reaction-layer thickness.
2. While monolithic fracture-mechanics solutions are useful for screening purposes, they fail to accurately capture the importance of the thickening of the oxide layer during the test and its effect on the driving force for crack advance and final failure.
3. The thickness of the oxide layer is a critical parameter in the mechanics of the reaction-layer fatigue mechanism. In the present case of polysilicon, the native oxide at the root of the notched cantilever-beam fatigue structure must exceed 2.9 nm in order to initiate cracks by a moisture-induced cracking mechanism and must exceed 46.4 nm to allow catastrophic failure at stresses below the strength of the polycrystalline silicon. This implies that it is possible to initiate cracks within the oxide layer that cannot propagate to failure, unless the oxide layer itself thickens throughout the test.
4. Interfacial fracture mechanics establish that a sufficiently thick reaction layer is required for the fracture toughness of the material to be exceeded.
5. Oxidation and cracking of the reaction layer lead to similar changes in the compliance of the notched, cantilever-beam fatigue characterization structure; this severely complicates the quantification of the time-dependence of reaction-layer fatigue.

Acknowledgements

This work was funded by the Director, Office of Science, Office of Basic Energy Research, Division of Materials Sciences and Engineering of the U.S. Department of Energy under Contract No. DE-AC03-76SF00098. Additional funding for equipment was provided by the New

Energy and Industrial Technology Development Organization (NEDO), Tokyo, Japan. The authors wish to thank Dr S.B. Brown of Exponent, Inc., Natick, MA, for his initial support, Dr W. Van Arsdell for the original specimen design, and Dr Eric Stach and Prof. Roger Howe for helpful discussions.

References

Allameh, S.M., Gally, B., Brown, S. and Soboyejo, W.O. (2001). *Surface Topology and Fatigue in Si MEMS Structures* (edited by Muhlstein, C. and Brown, S.), vol. 1413. Mechanical Properties of Structural Films, STP 1412. American Society for Testing and Materials, West Conshohocken, PA, 3–16.

Anderson, T.L. (1995). *Fracture Mechanics: Fundamentals and Applications*, 2nd ed. CRC Press, Boca Raton.

Bagdahn, J. and Sharpe, W.N.J. (2002). *Reliability of Polycrystalline Silicon Under Long-Term Cyclic Loading*, MEMS 2002. IEEE, Las Vegas, 447–450.

Beuth, J.L., Jr., (1992). Cracking of thin bonded films in residual tension. *International Journal of Solids and Structures* **29**, 1657–1675.

Broek, D. (1986). *Elementary Engineering Fracture Mechanics*, 4th ed. Kluwer Academic Publishers, Dordrecht, Holland.

Brown, S.B., Van Arsdell, W. and Muhlstein, C.L. (1997). Materials reliability in MEMS devices. In: *Proceedings of International Solid State Sensors and Actuators Conference (Transducers '97)* (edited by Senturia, S.), IEEE, Chicago, IL, U.S.A. 591–593.

Connally, J.A. and Brown, S.B. (1992). Slow crack growth in single-crystal silicon. *Science* **256**, 1537–1539.

Dundurs, M.R. (1969). Edge-bonded dissimilar orthogonal elastic wedges. *Journal of Applied Mechanics* **36**, 650–652.

Ford, F.P. and Silverman, M. (1979). *Mechanistic Aspects of Environment-Controlled Crack Propagation in Steel/Aqueous Environment Systems*, HTGE-451-8-12, General Electric Company.

Forsythe, G.E., Malcolm, M.A. and Moler, C.B. (1977). *Computer Methods for Mathematical Computations*. Prentice-Hall, Englewood Cliffs, NJ.

Gecit, M.R. (1979). Fracture of a surface layer bonded to a half space. *International Journal of Engineering Science* **17**, 287–295.

He, M.-Y. and Hutchinson, J.W. (1989). Crack deflection at an interface between dissimilar elastic materials. *International Journal of Solids and Structures* **25**, 1053–1067.

Hutchinson, J.W. and Suo, Z. (1992). Mixed Mode Cracking in Layered Materials. *Advances in Applied Mechanics* **29**, 63–163.

Jaeger, R.C. (1993). *Introduction to Microelectronic Fabrication* (edited bu V., Neudeck, G.W. and Pierret, R.F.), Modular Series on Solid State Devices, Addison-Wesley, New York.

Kahn, H., Ballarini, R., Mullen, R.L. and Heuer, A.H., (1999). Electrostatically actuated failure of microfabricated polysilicon fracture mechanics specimens. *Proceedings of the Royal Society of London* **A455**, 3807–3823.

Kapels, H., Aigner, R. and Binder, J. (1999). Fracture strength and fatigue of polysilicon determined by a novel thermal actuator [MEMS]. In: *Proceedings of the 29th European Solid-State Device Research Conference*. Leuven, Belgium. IEEE, Chicago, IL, 1522–1528.

Komai, K., Minoshima, K. and Inoue, S. (1998). Fracture and fatigue behavior of single crystal silicon microelements and nanoscopic AFM damage evaluation. *Microsystem Technologies* **5**, 30–37.

Michalske, T.A. and Freiman, S.W. (1983). A molecular mechanism for stress corrosion in vitreous silica. *Journal of the American Ceramic Society* **66**, 284–288.

Muhlstein, C.L., Brown, S.B. and Ritchie, R.O. (2001a). High-cycle fatigue and durability of polycrystalline silicon films in ambient air. *Sensors and Actuators* **A94**, 177–188.

Muhlstein, C.L., Brown, S.B. and Ritchie, R.O. (2001b). High-cycle fatigue of single crystal silicon thin films. *Journal of Microelectromechanical Systems* **10**, 593–600.

Muhlstein, C.L., Howe, R.T. and Ritchie, R.O. (2003). Fatigue of polycrystalline silicon for microelectromechanical systems applications: crack growth and stability under resonant loading conditions. *Mechanics of Materials*, **35**.

Muhlstein, C.L., Stach, E.A. and Ritchie, R.O. (2002a). Mechanism of fatigue in micron scale films of polycrystalline silicon for microelectromechanical systems. *Applied Physics Letters* **80**, 1532–1534.

Muhlstein, C.L., Stach, E.A. and Ritchie, R.O. (2002b). A reaction-layer mechanism for the delayed failure of micron-scale polycrystalline silicon structural films subjected to high-cycle fatigue loading. *Acta Materialia* **50**, 3579–3595.

Newman, R.C., Shahrabi, T. and Sieradzki, K. (1989). Film-induced cleavage of alpha-brass. *Scripta Metallurgica* **23**, 71–74.

Pugh, E.N. (1985). Progress toward understanding the stress corrosion problem. *Corrosion* **41**, 517–526.

Simmons, G. and Wang, H. (1971). *Single Crystal Elastic Constants and Calculated Aggregate Properties: a Handbook*, 2nd ed. M.I.T. Press, Cambridge, MA.

Tabib-Azar, M., Wong, K. and Wen, K. (1992). Aging phenomena in heavily doped (p/sup +/) micromachined silicon cantilever beams. *Sensors and Actuators A* **A33**, 199–206.

Tada, H., Paris, P.C. and Irwin, G.R. (2000). *The Stress Analysis of Cracks Handbook*, 3rd ed. ASME Press, New York.

Tatsumi, Y. and Ohsake, H. (1988). *Properties of Silicon*. IEE, London, U.K., 3–6.

Van Arsdell, W.W. and Brown, S.B. (1999). Subcritical crack growth in silicon MEMS. *Journal of Microelectromechanical Systems* **8**, 319–327.

Ye, T., Suo, Z. and Evans, A.G. (1992). Thin film cracking and the roles of substrate and interface. *International Journal of Solids and Structures* **29**, 2639–2648.

Zak, A.R. and Williams, M.L. (1963). Crack point singularities at a bimaterial interface. *Journal of Applied Mechanics* **30**, 142–143.